Nuclear Science and Techniques (2025) 36:50
https://doi.org/10.1007/s41365-025-01663-x

Selection of abnormal trends in nuclear β-decay half-lives by neural network and exploration of the physical mechanisms

Peng Li[1,2] · **Zhong-Ming Niu**[3] · **Yi-Fei Niu**[1,2]

Received: 29 September 2024 / Revised: 15 December 2024 / Accepted: 20 December 2024 / Published online: 13 February 2025

Abstract

Nuclear β-decay, a typical decay process for unstable nuclei, is a key mechanism for producing heavy elements in the Universe. In this study, neural networks were employed to predict β-decay half-lives and, for the first time, to identify abnormal trends in nuclear β-decay half-lives based on deviations between experimental values and the predictions of neural networks. Nuclei exhibiting anomalous increases, abrupt peaks, sharp decreases, abnormal odd-even oscillations, and excessively large experimental errors in their β-decay half-lives, which deviate from systematic patterns, were identified through deviations. These anomalous phenomena may be associated with shell effects, shape coexistence, or discrepancies in the experimental data. The discovery and analysis of these abnormal nuclei provide a valuable reference for further investigations using sophisticated microscopic theories, potentially offering insights into new physics through studies of nuclear β-decay half-lives.

Keywords β-decay half-lives · Neural network · Abnormal nuclei

1 Introduction

"How were the elements from iron to uranium made?" This is a highly fascinating question and has been listed in "Connecting Quarks with the Cosmos: Eleven Science Questions for the New Century" [1]. Rapid neutron capture processes (r-process) are responsible for producing approximately half of these heavy elements [2, 3] and represent the only mechanism for synthesizing elements heavier than bismuth [4]. One of the key challenges in studying the r-process is obtaining precise nuclear physics inputs, such as nuclear masses, β-decay half-lives, neutron-capture cross-sections, and fission rates [5]. β-decay, the primary decay mode for most nuclei, plays a crucial role in determining the timescale of the r-process. Predictions indicate that there are 9035 bound nuclides with proton numbers between 8 and 120 [6]. However, only approximately 3,000 nuclides have been observed experimentally [7]. In particular, for nuclei far from the β-stability line—those most relevant to the r-process—current experimental data remain limited. Theoretical calculations not only guide experimental observations but also provide explanations for existing experiments, thereby advancing a deeper understanding of the essence of matter and the laws of nature. Nevertheless, providing a precise description of the β-decay half-lives of nuclei remains a significant challenge owing to the non-perturbative nature of nuclear forces and the complexity of quantum many-body problems.

Theoretical studies on β-decay half-lives can be broadly classified into empirical formulas, gross theories, and microscopic theories. The empirical formula is particularly suitable for fitting experimental data and calculating β-decay half-lives on a large scale [8, 9]. Compared to empirical formulas, gross

This work was partly supported by the 'Young Scientist Scheme' of the National Key R&D Program of China (No. 2021YFA1601500), National Natural Science Foundation of China (Nos. 12075104, 12375109, 11875070, and 11935001), Anhui Project (Z010118169), and Key Research Foundation of the Education Ministry of Anhui Province (No. 2023AH050095).

✉ Zhong-Ming Niu
zmniu@ahu.edu.cn

✉ Yi-Fei Niu
niuyf@lzu.edu.cn

1 School of Nuclear Science and Technology, Lanzhou University, Lanzhou 730000, China

2 Frontiers Science Center for Rare Isotopes, Lanzhou University, Lanzhou 730000, China

3 School of Physics and Optoelectronic Engineering, Anhui University, Hefei 230601, China

theory can handle more complex situations and offers broader applicability [10–13]. Microscopic theories include the shell model [14–18] and the quasiparticle random phase approximation (QRPA) model [19–29]. The shell model provides reliable predictions for β-decay half-lives, particularly for nuclei in the light nuclear region and near magic numbers. However, shell model calculations become increasingly challenging as the number of valence nucleons increases. QRPA, on the other hand, is widely used to calculate the β-decay properties of the majority of nuclei on the nuclear chart, with the exception of some light nuclei. When experimental data are unavailable, researchers frequently rely on QRPA predictions based on the finite-range droplet model (FRDM + QRPA) [30–33] to provide essential inputs for *r*-process simulations.

In recent years, with rapid advancements in artificial intelligence, machine learning has provided researchers with novel approaches. The application of machine learning in the field of nuclear physics has become increasingly prominent [34], with applications spanning various areas, including nuclear mass predictions [35–41], investigations of charge radii [42–47], predictions of the distribution of fission fragment yields [48, 49], studies of giant dipole resonances [50, 51], explorations of excited states [52, 53], and other relevant topics [54–63].

The use of machine learning to study β-decay half-lives has also garnered significant attention in recent years, with predictive accuracy continually improving [64–68]. Recent studies demonstrated that machine learning predictions for β-decay half-lives deviate from experimental values by only 2.24 times for nuclei with half-lives shorter than 10^6 seconds [67]. In this study, we propose a novel application of neural networks to identify nuclei exhibiting deviations from systematic behavior in β-decay half-lives. For these nuclei, machine learning fails to accurately describe the β-decay half-lives. Furthermore, theoretical models such as FRDM+QRPA [32, 33], relativistic Hartree–Bogoliubov + quasiparticle random phase approximation (RHB+QRPA) [26], gross theory based on the WS4 mass model (WS4+GT) [13], and Skyrme–Hartree–Fock–Bogoliubov with the finite amplitude method (SHFB+FAM) [69] also encounter difficulties in describing these specific nuclei. After predicting β-decay half-lives and selecting these anomalous nuclei based on deviations between experimental values and neural network predictions, we analyzed the challenges faced by the neural network in describing these nuclei and explored the potential underlying physics.

2 Neural network model

In this study, the neural network employed (Z, N, Q_β) as inputs to predict β-decay half-lives and identify abnormal nuclei based on deviations between experimental values and neural network predictions. Here, Z, N, and Q_β represent the proton number, neutron number, and β-decay energy, respectively. The Q_β values were calculated using nuclear masses obtained from the Bayesian machine learning (BML) model [37], which achieves a root-mean-square error (RMSE) of only 84 keV compared to experimental values. The neural network output corresponds to the logarithm of the β-decay half-life ($\log_{10} T_{1/2}$).

A total of 1,072 nuclei from the NUBASE2020 database [7] were selected based on the following criteria: $Z \geq 8$, $N \geq 8$, β-decay half-lives shorter than 10^6 seconds, and β-decay branching ratios greater than 10%. Consequently, the predicted β-decay half-lives from the neural network were all less than 10^6 seconds. The experimental values for most of these 1072 nuclei were highly precise; for instance, the RMSE between the upper limits of experimental values and their means was calculated to be only 0.056 orders of magnitude, which is significantly lower than the deviations observed in both the neural network and theoretical models. This indicates that the larger deviations occur in isolated cases, primarily in a few specific nuclei, and highlights the need for more precise measurements in future experiments. To validate the model, a process akin to fivefold cross-validation was employed. The dataset was randomly shuffled and divided into five parts, containing 214, 214, 214, 214, and 216 nuclei, respectively. In each iteration, one part served as the validation set, while the remaining four parts constituted the training set. This process was iteratively repeated, which ensured that each nucleus was represented equally in both training and validation sets. This methodology differs from the neural networks employed in [67]. Five datasets were generated in this manner. Each dataset was trained for 20,000 iterations, selecting the best 20 models per dataset, resulting in 100 models. During training, different weight matrices were initialized from a truncated normal distribution $\mathcal{N}(0, \sqrt{2/(h_{\mathrm{in}} + h_{\mathrm{out}})})$, where h_{in} and h_{out} represent the number of neurons at the input and output ends of the weight matrix, respectively [70]. Each training session utilized a different initial weight matrix and ran for 50,000 iterations. The uncertainties in the neural network predictions arise from variations in these initial weight matrices. The mean of the predictions from the 100 models was taken as the result of ANN1, while the standard deviation represented the uncertainty in the neural network predictions. Additionally, a Bayesian neural network (BNN) approach could be employed to provide unequally weighted uncertainties, yielding only slight differences from the uncertainties obtained in this study. These differences did not affect the primary conclusions. The root-mean-square uncertainty $\sigma_{\mathrm{rms}}(\log_{10} T_{1/2})$ for ANN1 was calculated across various half-life intervals.

$$\sigma_{\rm rms}(\log_{10} T_{1/2}) = \sqrt{\frac{\sum_{i=1}^{n}(\log_{10} T_{1/2}^{\rm Exp} - \log_{10} T_{1/2}^{\rm ANN1})^2}{n}}. \quad (1)$$

To identify abnormal nuclei in the neural network, nuclei with different orders of magnitude of β-decay half-lives were analyzed. Abnormal nuclei were defined as those where the neural network predictions deviated from experimental values by more than 1.96 times the root-mean-square uncertainty $\sigma_{\rm rms}(\log_{10} T_{1/2})$, corresponding to a 95% confidence interval. Using this criterion, 70 abnormal nuclei were identified. These nuclei were subsequently excluded from the dataset, and the remaining 1002 nuclei underwent the same fivefold cross-validation procedure as that employed for ANN1, resulting in the predictions for ANN2.

In this study, a double-hidden-layer neural network was used, which is described by the following formula:

$$\boldsymbol{h}_j^{[1]} = \text{softsign}\left(\sum_{i=1}^{n} \boldsymbol{\omega}_{ij}^{[1]}\boldsymbol{x}_i + \boldsymbol{b}_j^{[1]}\right), \quad (2)$$

$$\boldsymbol{h}_k^{[2]} = \text{softsign}\left(\sum_{j=1}^{H_1} \boldsymbol{\omega}_{jk}^{[2]}\boldsymbol{h}_j^{[1]} + \boldsymbol{b}_k^{[2]}\right), \quad (3)$$

$$y = 6 \times \tanh\left(\sum_{k=1}^{H_2} \boldsymbol{\omega}_k^{[3]}\boldsymbol{h}_k^{[2]} + b^{[3]}\right). \quad (4)$$

Here, $\boldsymbol{x}$ represents the inputs, $\boldsymbol{\omega}$ and $\boldsymbol{b}$ denote the weight matrix and bias term, respectively, and $\boldsymbol{h}$ indicates the hidden layer matrix. The parameters $H_1 = 29$ and $H_2 = 2$ specify the number of neurons in the first and second hidden layers, respectively, while y represents the output. To ensure consistency with the FRDM+QRPA, RHB+QRPA, SHFB+FAM, and WS4+GT models, which predicted half-lives greater than 10^{-4} s for almost all nuclei, the predictive range of the neural network was extended to include β-decay half-lives greater than 10^{-6} s.

After calculating the output value y for each input, the loss function Loss is determined as follows:

$$\text{Loss} = \frac{\sum_{i=1}^{m}(y_{\rm Exp} - y_{\rm Pre})^2}{m} + \frac{\lambda}{2}\sum_j \boldsymbol{\theta}_j^2, \quad (5)$$

where $y_{\rm Exp}$ represents the experimental value from NUBASE2020, while $y_{\rm Pre}$ denotes the predictions of the neural network. The parameters of the neural network, including the weight matrix $\boldsymbol{\omega}$ and bias term $\boldsymbol{b}$, are collectively represented by $\boldsymbol{\theta}$. The variable m specifies the number of data points in the training set, and λ is the hyperparameter for L_2 regularization (Tikhonov regularization [71, 72]). This regularization term helps to prevent the neural network from overfitting, marking an improvement over the methodology used in [67].

3 Results and discussion

Figure 1 presents the RMSE values for the predictions of the ANN1 and ANN2 models across various half-life ranges. To facilitate a clearer comparison between ANN1 and ANN2, the RMSE values for ANN1, excluding the abnormal nuclei, are also shown. The results indicate that in most cases, the performance differences between the two neural networks on both the training and validation sets are minimal, suggesting that neither model suffers from overfitting. Furthermore, Fig. 1 demonstrates that the predictive accuracy of the neural network generally improves as nuclear half-lives decrease, except for nuclei with half-lives in the ranges of $10^{-2} \sim 10^{-1}$ to $10^{-3} \sim 10^{-2}$ s. For a clearer comparison of the ANN1 and ANN2 predictions, the RMSE values for ANN1, with abnormal nuclei excluded, are presented. Notably, ANN1, when the selected 70 abnormal nuclei are excluded, achieves prediction accuracy comparable to that of ANN2. This consistency suggests that the selected abnormal nuclei exhibit behavior distinct from that of other nuclei.

Figure 2 illustrates typical abnormal nuclei identified by the neural networks. The predicted β-decay half-lives for nuclei in isotopic chains exhibit a generally smooth decrease as they move further from the β-stability line, consistent with experimental data. To improve predictions of β-decay half-lives, additional physical parameters were introduced alongside the inputs (Z, N, Q_β). These included the odd-even information δ ($\delta = (-1)^Z/2 + (-1)^N/2$), the deformation parameter β_2, and a variable related to magic numbers P ($P = \nu_p\nu_n/(\nu_p + \nu_n)$ where ν_p and ν_n are the differences between Z, N and their nearest magic numbers). However, incorporating these parameters did not significantly improve predictions for the abnormal nuclei, and extrapolations were less accurate than the results presented. Figure 2 demonstrates that the identified nuclei exhibit various anomalous behaviors. For example, (1) Anomalous increases: with the neutron number increases, certain nuclear half-lives show a notable rise, such as nuclei ranging from ^{32}Al to ^{36}Al. (2) Sharp decreases: compared to surrounding nuclei, some nuclei exhibit a marked decrease in half-lives compared to their neighbors, such as ^{64}Co and ^{98}Zr. (3) Excessively large experimental errors: for some nuclei, experimental measurements of their half-lives come with relatively large uncertainties, such as ^{36}Al and ^{74}Fe. (4) Abnormal odd-even oscillations: for specific nuclei, their β-decay half-lives exhibit odd-even oscillations distinct from typical patterns, such as ^{104}Tc. (5) Abrupt peaks: some nuclei demonstrate sudden peaks in their half-lives, making them stand out, such as

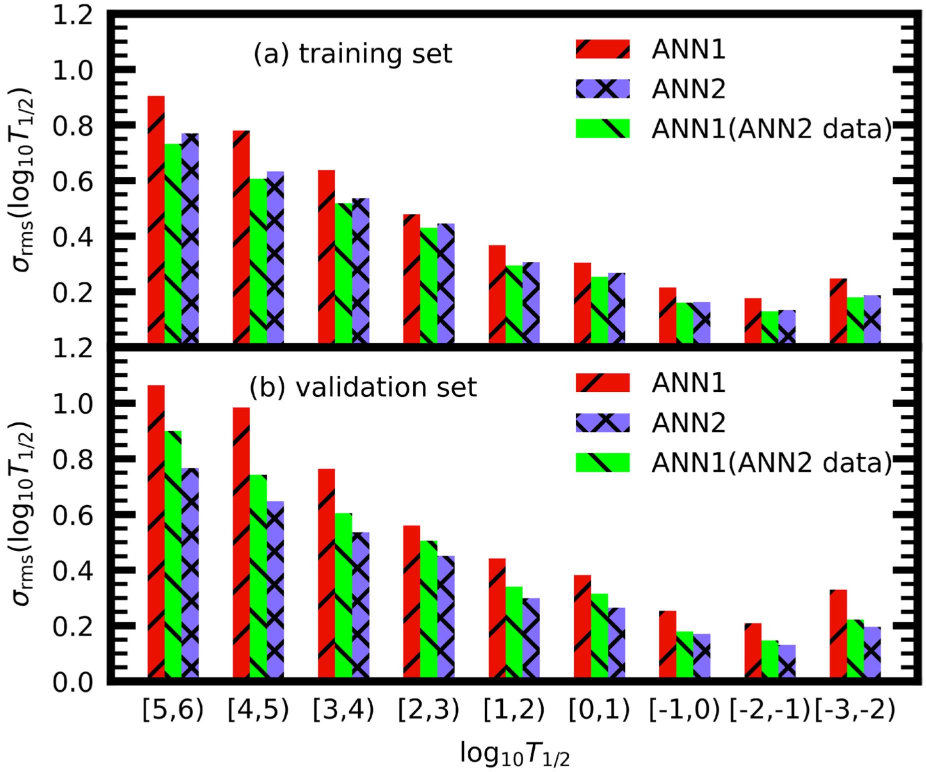

Fig. 1 (Color online) The root-mean-square deviation, $\sigma_{\rm rms}(\log_{10} T_{1/2})$, was calculated across different half-life magnitudes to compare the predicted β -decay half-lives with experimental values. These results were evaluated for both the training set (a) and validation set (b). Each bar in the comparison represents the outcomes for three cases: ANN1 applied to the entire dataset, ANN2 applied to the dataset excluding abnormal data, and ANN1 applied to the dataset excluding abnormal data

^{70}Co and ^{36}Al. The ANN1 predictions for nuclei such as ^{28}Al, ^{106}Tc, and ^{47}Ca also showed significant deviations due to the higher RMSE of ANN1 for nuclei with longer half-lives. However, these deviations remained within 1.96 times the RMSE for their intervals, meaning these nuclei were not classified as abnormal.

For these nuclei, the predictions from the machine learning models exhibited significant discrepancies when compared with the experimental data. However, accurately describing these isotopes remains a challenge even when employing other theoretical models. For the Al isotopes, the FRDM+QRPA model can accurately predict the β-decay half-lives of ^{31}Al and ^{32}Al but shows a significant deviation in predicting the β-decay half-lives of ^{33}Al to ^{36}Al compared to the experimental data. On the other hand, RHB+QRPA offers more accurate predictions for the β-decay half-lives of ^{34}Al to ^{36}Al but shows notable discrepancies when predicting the β-decay half-lives of other nuclei in the isotopic chain. Both models fail to reproduce the observed trend of anomalous increases in β-decay half-lives from ^{32}Al to ^{36}Al. For the Co isotopes, RHB+QRPA provides better predictions for the β-decay half-life of ^{70}Co when compared to the neural network, although, for other nuclei in this isotopic chain, its predictive accuracy is lower than that of the neural networks. The FRDM+QRPA model shows better agreement with the experimental data for nuclei lighter than ^{66}Co compared to the neural networks; however, for nuclei heavier than ^{67}Co, its predictions are less accurate than those of the neural networks. Moreover, predicting the β-decay half-life of ^{70}Co using FRDM+QRPA remains particularly challenging. Both models also struggle to reliably predict the β-decay half-lives of all the nuclei in the Co isotopes. For the other isotopes selected in Fig. 2, neither the FRDM+QRPA nor the RHB+QRPA models are able to accurately reproduce the β-decay half-lives of the abnormal nuclei or their neighboring nuclei.

In Fig. 3, the extrapolation results of two models are presented, accompanied by the 1σ (68% confidence interval) error bands. From Fig. 3, for nuclei with measured half-lives, the error bands of the neural network are small, indicating good agreement with the experimental data. For the nuclei selected by the neural network based on deviations between the experimental values and the predictions, both neural network models provide consistent results. Benefiting from training on an abnormal dataset, ANN1 achieved slightly improved predictive performance. However, neither model can precisely describe these abnormal nuclei. For nuclei without experimental values, ANN1 exhibits larger error bands. For all nuclei, the RMS between the means/upper bound/lower bound of ANN1 and ANN2 were 0.115, 0.196, and 0.162 orders of magnitude, respectively, which are very close, with the predictions of ANN1 being slightly shorter than those of ANN2 in some cases.

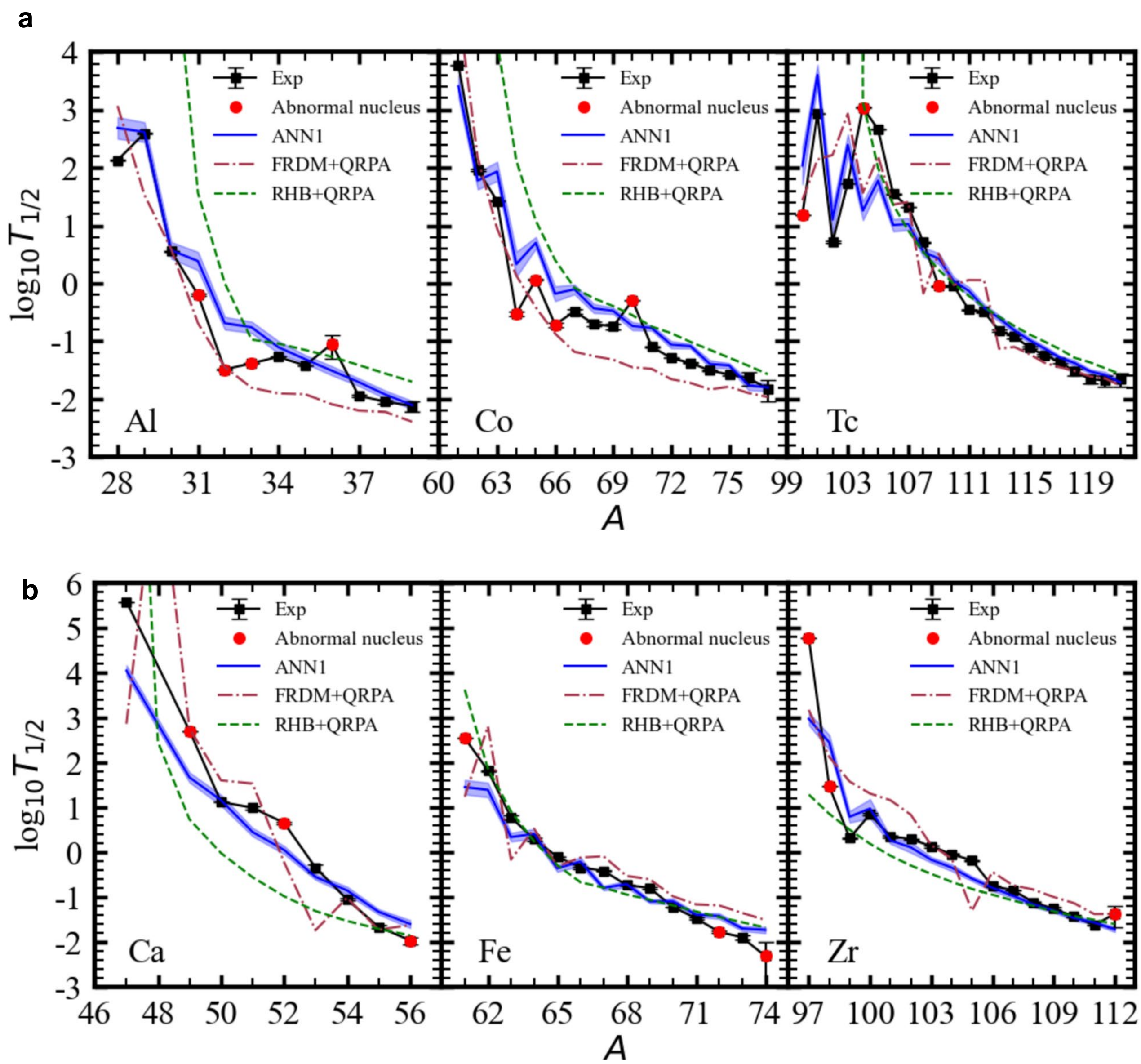

Fig. 2 (Color online) The nuclear β-decay half-lives predicted by the neural network ANN1 are shown for the odd isotopes Al, Co, and Tc, as well as the even isotopes Ca, Fe, and Zr, along with their corresponding 68% confidence interval error bars. The red points represent the abnormal nuclei identified by ANN1. For comparison, theoretical predictions from the RHB + QRPA and FRDM + QRPA models are also included

Figure 4 compares the β-decay half-lives of isotones predicted by ANN2 and other theoretical models. For nuclei with experimental data, the predictions of the neural network show better agreement with the experimental results than those of other theoretical models. For the selected dataset of 1072 nuclei, the RMSE between the predictions of ANN1 and the experimental values was 0.437, while the FRDM+QRPA model shows an RMSE of 0.806. Since the predictions of RHB+QRPA for some of the 1072 nuclei were stable, the RMSE for RHB+QRPA predictions for nuclei with half-lives shorter than 10^6s was 1.025 for a subset of 920 nuclei. Compared to these theoretical models, the neural network demonstrates higher predictive accuracy for β-decay half-lives. The neural network predicts shorter half-lives than those predicted by other theoretical models in the neutron-rich region of $N = 50$ isotones. However, in the neutron-rich regions of $N = 82$ and 126 isotones, the predictions from the neural network align more closely with those from the other theoretical models, showing less disagreement.

Figure 5 shows the logarithmic differences between the β-decay half-lives predicted by ANN1 and the experimental

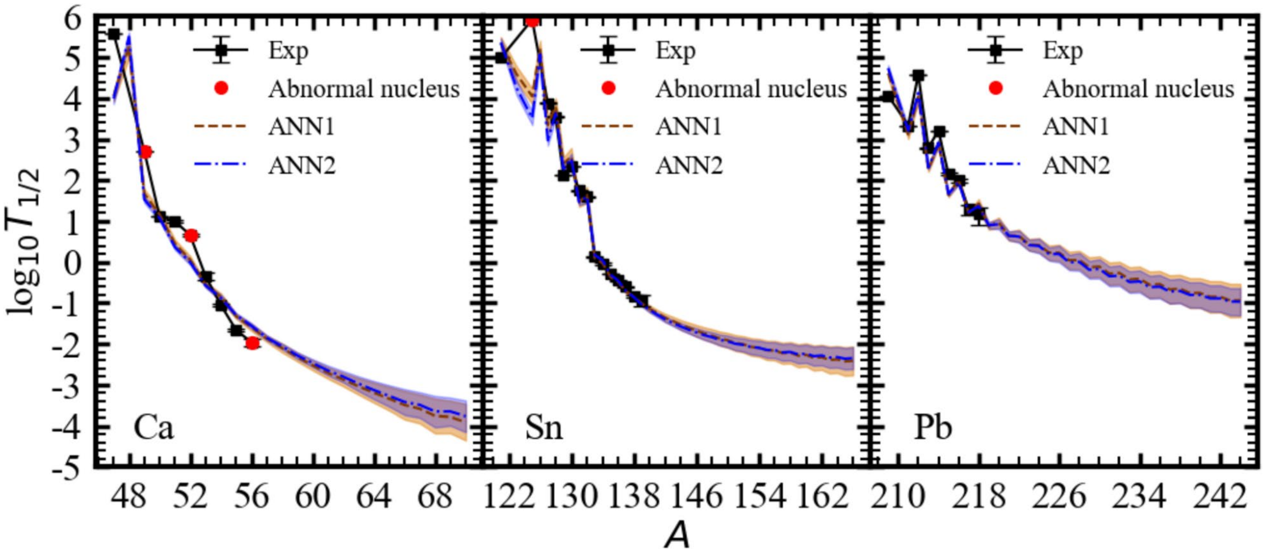

Fig. 3 (Color online) Nuclear β-decay half-lives predicted by neural networks ANN1 and ANN2 for the Ca, Sn, and Pb isotopes are presented along with the corresponding 68% confidence interval error bars. The abnormal nuclei identified by the networks are highlighted by red points. Experimental β-decay half-lives from NUBASE2020 are also included for comparison

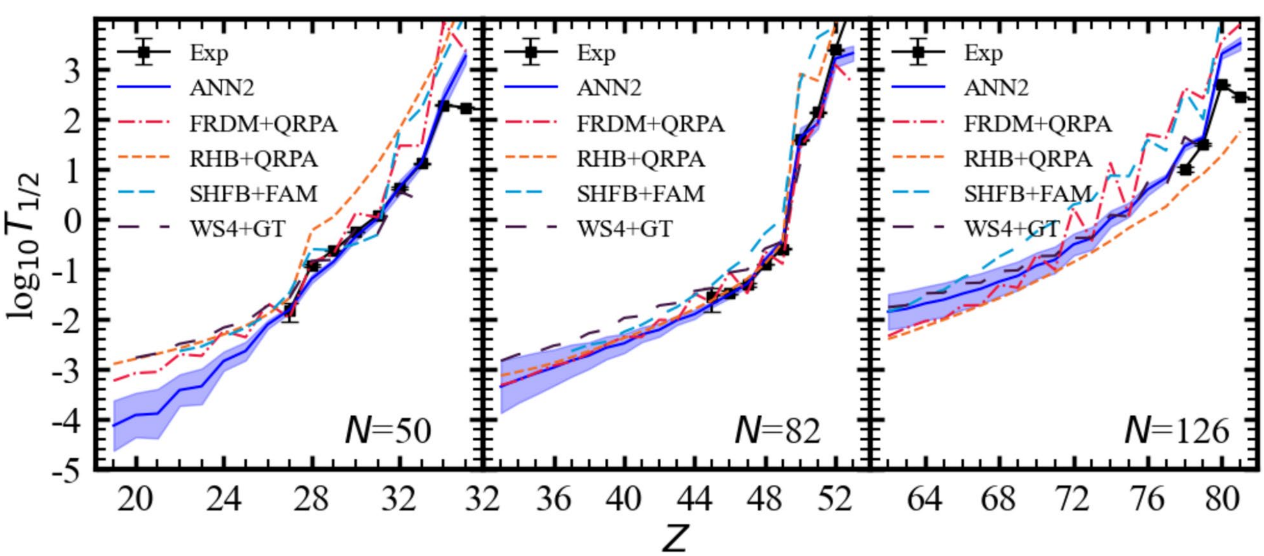

Fig. 4 (Color online) β-decay half-lives of isotones predicted by ANN2 in comparison with the FRDM+QRPA, RHB+QRPA, SHFB+FAM, and WS4+GT results

values from NUBASE2020 for the 1072 nuclei selected in the dataset. The figure indicates that nuclei with significant deviations between the predictions of ANN1 and experimental values are concentrated near the β-stability line. For most nuclei (75.2%), the deviation between the predictions of ANN1 and the experimental values was within 0.4 orders of magnitude. Among the 1072 β-decay half-lives, 548 (51.1%) were overestimated, and 524 (48.9%) were underestimated by ANN1. ANN1 exhibited alternating blocks of overestimation and underestimation in predicting the β-decay half-lives of the nuclei, accompanied by a certain degree of randomness. Neural networks tend to underestimate the β-decay half-life of nuclei with magic numbers. For nuclei with magic numbers of protons or neutrons, 52 (58.4%) were underestimated, and 37 (41.6%) were overestimated by ANN1. This suggests that the greater stability of magic nuclei presents additional challenges for neural networks in predicting their β-decay half-lives.

In Fig. 6, a concise analysis is provided to explain why the neural network faces challenges in predicting certain

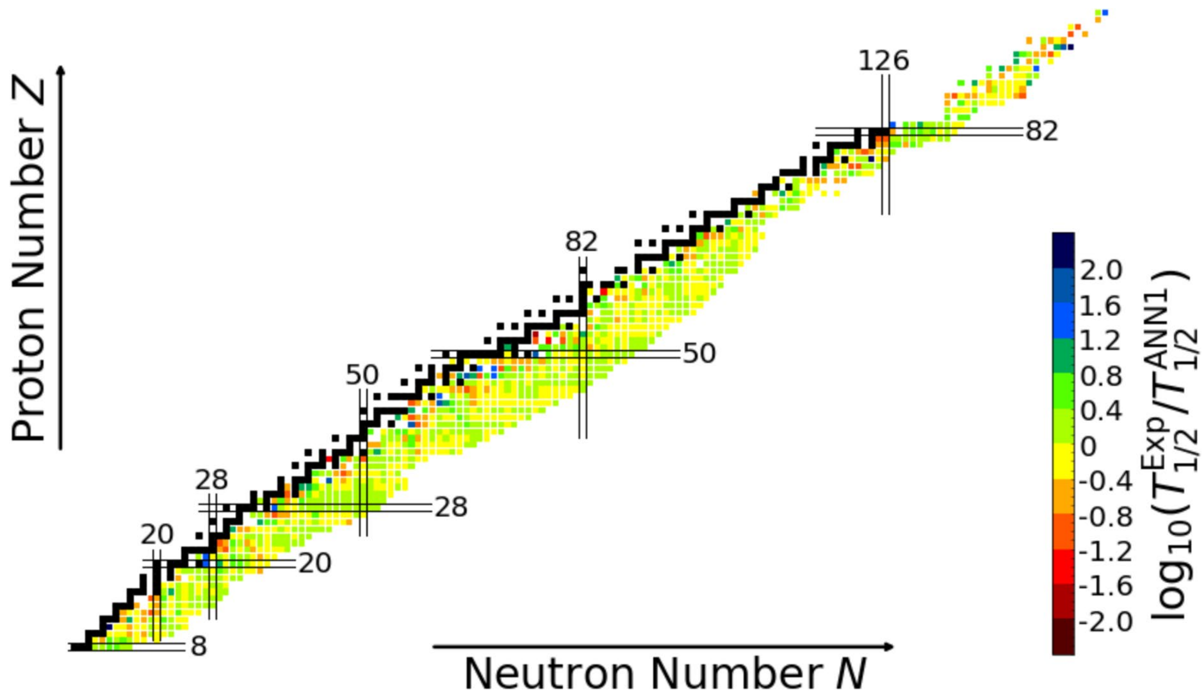

Fig. 5 (Color online) The logarithmic difference distribution of β-decay half-lives between the predictions by ANN1 and experimental values on the nuclear chart is shown, with black squares representing stable nuclei

nuclei. For ^{52}Ca, both the predictions from the WS4 model and the experimental values reveal a significant Δ_{2n} value ($\Delta_{2n} = S_{2n}(Z,N) - S_{2n}(Z,N+2)$, where S_{2n} is the two-neutron separation energy), indicating the presence of shell effects. A recent study also identified $N = 32$ as a new magicity [74]. However, our neural network model does not incorporate this information, which leads to reduced predictive accuracy for nuclei in this region. For ^{112}Zr, the experimental half-life measurements have relatively large uncertainties, resulting in different outcomes depending on how the error bars are treated. For instance, NUBASE2020 reports a half-life of 43 ± 21 ms using symmetric error bars, while the original measurement of the β-decay half-life for this nucleus was 30^{+20}_{-10} ms [75]. Future experimental measurements with smaller error bars would help resolve this issue. For ^{97}Zr, ^{98}Zr, and ^{104}Tc, the β_2 data provided by the FRDM+QRPA and WS4 models [76] for nuclei in their vicinity show notable discrepancies, suggesting possible shape coexistence in these nuclei. This may explain the difficulties encountered by our neural network in predicting nuclei in this region. The β-decay half-lives of these abnormal nuclei, which deviate from systematic patterns, may be better understood through future in-depth investigations using more sophisticated models. Such studies could uncover new physics, thereby advancing our understanding of nuclear β-decay.

The selected nuclei are listed in Table 1 along with their experimental half-lives and predictions from ANN1 and ANN2. The abnormal nuclei include 32 odd-odd nuclei, 26 odd-A nuclei, and 12 even-even nuclei. Owing to the presence of unpaired nucleons in odd nuclei, these exhibit complex energy-level structures, vibrational modes, and other properties, making theoretical descriptions more challenging. While neural networks outperform traditional nuclear models in their representation capabilities, their performance is somewhat worse when dealing with odd nuclei compared to even nuclei. This highlights the vital role of physics in enhancing the performance of machine learning algorithms.

4 Summary and outlook

In this study, a neural network was employed to predict β-decay half-lives and to identify nuclei whose β-decay half-lives deviated from systematic patterns, based on the differences between experimental values and the neural network predictions. After excluding these anomalous data points, the models were retrained. Both neural network models exhibited similar $\sigma_{\mathrm{rms}}(\log_{10} T_{1/2})$ values, with the model trained on the original dataset showing slightly larger error bands when extrapolated into the region of lighter nuclei. A brief analysis was also conducted to

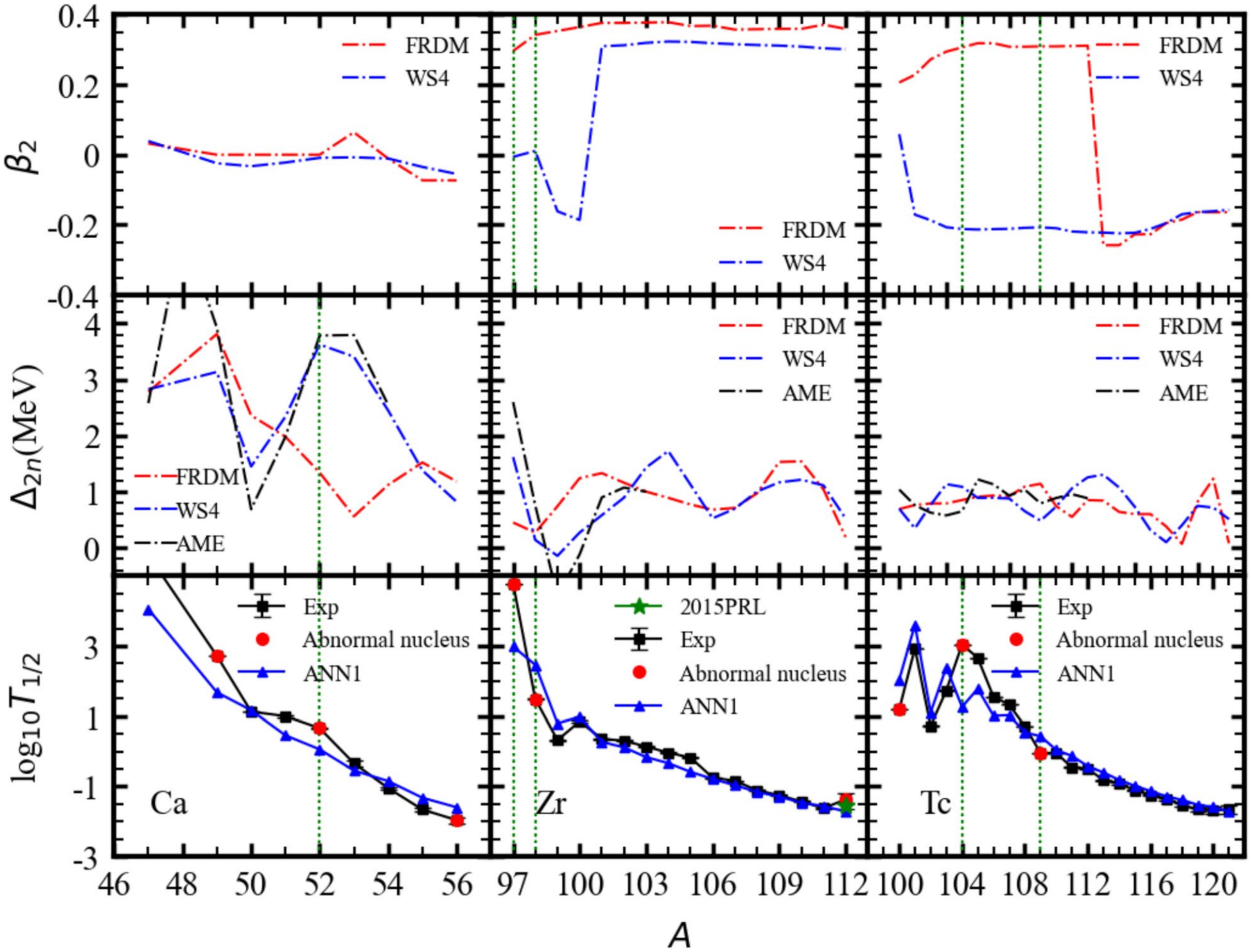

Fig. 6 (Color online) The predictions of ANN1 and the experimental values of $\log_{10} T_{1/2}$ for the Ca, Zr, and Tc isotopes, including abnormal nuclei, are shown, along with the quadrupole deformation parameter β_2 from the FRDM and WS4 models. Additionally, the two-neutron shell gap values, Δ_{2n}, from the FRDM and WS4 predictions, as well as the experimental values from AME [73], are provided

investigate the factors contributing to the challenges in predicting the half-lives of the selected nuclei. These challenges were found to be linked to the structural characteristics of the nuclei, which the neural network did not account for. In the future, more sophisticated microscopic theoretical studies could provide a deeper understanding of these abnormal nuclei, further advancing our comprehension of β-decay. Incorporating more relevant input parameters into the neural network could enhance its capability to predict β-decay half-lives more effectively. Furthermore, it may be beneficial to sample the experimental values using a probability distribution function from the training dataset. While this method was not employed in this study owing to the high precision of the experimental β-decay half-lives, we believe it could be valuable in future nuclear physics research. Neural networks were used to directly learn from experimental values of nuclear β-decay half-lives, taking known variables related to β-decay half-lives (Z, N, and Q_β) as inputs. This approach achieved high prediction accuracy for β-decay half-lives without considering other theoretical factors. The anomalies in β-decay half-lives identified through the neural network method represent currently unexplained phenomena, which may provide insights for discovering new physics in the future. Additionally, other machine learning methods, such as density-based spatial clustering of applications with noise (DBSCAN), K-nearest neighbors (KNN), and other algorithms, can also be applied to identify abnormal nuclei, potentially offering new perspectives on anomalous phenomena in nuclear β-decay half-lives. We hope that

Table 1 The selected nuclei exhibiting abnormal trends in nuclear β-decay half-lives, as identified by the neural network, are listed along with their experimental β-decay half-lives and the corresponding predictions from ANN1 and ANN2

Z	N	$\log_{10}(T_{1/2}^{\mathrm{Exp}})$	$\log_{10}(T_{1/2}^{\mathrm{ANN1}})$	$\log_{10}(T_{1/2}^{\mathrm{ANN2}})$	Z	N	$\log_{10}(T_{1/2}^{\mathrm{Exp}})$	$\log_{10}(T_{1/2}^{\mathrm{ANN1}})$	$\log_{10}(T_{1/2}^{\mathrm{ANN2}})$
9	13	0.626	−0.094	−0.467	33	48	1.522	2.272	2.384
9	15	−0.416	−1.200	−1.379	35	45	3.063	4.390	4.757
10	16	−0.706	−0.193	0.063	35	50	2.241	3.269	3.242
10	17	−1.510	−1.132	−1.105	40	57	4.780	2.983	2.936
10	18	−1.726	−1.198	−1.127	40	58	1.487	2.460	2.387
11	13	4.731	1.972	1.446	40	72	−1.367	−1.713	−1.687
11	16	−0.521	−0.042	0.040	41	57	0.456	1.456	1.699
11	17	−1.480	−1.121	−1.122	41	58	1.176	1.964	2.390
12	18	−0.499	0.051	0.445	42	63	1.560	0.820	0.752
12	20	−1.095	−0.743	−0.565	43	57	1.189	2.036	2.407
12	21	−1.036	−1.472	−1.338	43	61	3.041	1.261	0.922
13	18	−0.191	0.388	0.690	43	66	−0.043	0.432	0.388
13	19	−1.487	−0.686	−0.458	45	64	1.907	2.655	2.857
13	20	−1.382	−0.758	−0.517	45	65	0.525	1.411	1.153
13	23	−1.046	−1.509	−1.502	45	66	1.041	1.819	1.871
14	20	0.442	1.075	1.508	47	65	4.052	2.101	1.386
15	19	1.094	2.117	2.145	47	67	0.663	1.507	0.982
19	35	−2.000	−1.543	−1.508	47	69	2.361	1.090	0.861
20	29	2.719	1.678	1.537	50	75	5.920	4.046	3.512
20	32	0.663	0.060	0.000	51	83	−0.171	0.439	0.544
20	36	−1.959	−1.593	−1.555	52	77	3.621	5.005	5.330
21	35	−1.585	−1.101	−1.058	53	75	3.207	5.067	5.702
23	33	−0.666	−0.140	0.132	59	85	3.016	4.331	4.721
25	37	−1.036	−0.649	−0.473	75	119	0.699	1.315	1.420
26	35	2.555	1.461	1.399	77	119	1.716	2.451	2.769
26	46	−1.770	−1.414	−1.373	77	121	0.940	1.761	1.982
26	48	−2.301	−1.727	−1.671	77	122	0.845	1.742	1.914
27	37	−0.523	0.335	0.640	78	124	5.200	2.528	2.509
27	38	0.064	0.704	0.757	79	123	1.453	2.338	2.618
27	39	−0.712	−0.176	0.082	79	124	1.778	2.509	2.642
27	43	−0.294	−0.737	−0.658	81	125	2.402	3.485	3.697
28	37	3.957	2.658	2.211	81	126	2.457	3.525	3.648
29	39	1.490	2.287	2.436	87	146	−0.046	1.115	1.128
32	45	4.606	2.889	2.754	91	148	3.812	2.348	2.151
33	47	1.182	2.168	2.505	94	153	5.293	2.939	2.625

future work will explore more appropriate machine learning techniques for identifying abnormal nuclei.

Author Contributions All authors contributed to the study conception and design. Material preparation, data collection, and analysis were performed by Peng Li, Zhong-Ming Niu, and Yi-Fei Niu. The first draft of the manuscript was written by Peng Li, and all authors commented on previous versions of the manuscript. All authors read and approved the final manuscript.

Data Availability The data that support the findings of this study are openly available in Science Data Bank at https://cstr.cn/31253.11.sciencedb.j00186.00529 or https://doi.org/10.57760/sciencedb.j00186.00529.

Declarations

Conflict of interest The authors declare that they have no conflict of interest.

References

1. National Research Council, *in Connecting quarks with the cosmos: eleven science questions for the new century* (The National Academies Press, Washington, 2003)
2. M. Sasano, G. Perdikakis, R.G.T. Zegers et al., Gamow-Teller Transition Strengths from ^{56}Ni. Phys. Rev. Lett. **107**, 202501 (2011). https://doi.org/10.1103/PhysRevLett.107.202501
3. E. Margaret Burbidge, G. R. Burbidge, W. A. Fowler *et al.*, Synthesis of the elements in stars. Rev. Mod. Phys. **29**, 547 (1957). https://doi.org/10.1103/RevModPhys.29.547
4. F. Käppeler, R. Gallino, S. Bisterzo et al., The s process: Nuclear physics, stellar models, and observations. Rev. Mod. Phys. **83**, 157 (2011). https://doi.org/10.1103/RevModPhys.83.157
5. M. Arnould, S. Goriely, K. Takahashi, In-medium nuclear interactions of low-energy hadrons. Phys. Rep. **450**, 97 (2007). https://doi.org/10.1016/j.physrep.2007.08.002
6. X.W. Xia, Y. Lim, P.W. Zhao et al., The limits of the nuclear landscape explored by the relativistic continuum Hartree-Bogoliubov theory. At. Data Nucl. Data Tables **121–122**, 1 (2018). https://doi.org/10.1016/j.adt.2018.02.001
7. F.G. Kondev, M. Wang, W.J. Huang et al., The NUBASE2020 evaluation of nuclear physics properties. Chin. Phys. C **45**, 030001 (2021). https://doi.org/10.1088/1674-1137/abddae
8. Y. Zhou, Z. H. Li, Y. S. Chen *et al.*, Estimate of β^{-}-decay half-lives for *r*-process Nuclei, Nucl. Phys. Rev. **6034**, 425 (2017). https://doi.org/10.11804/NuclPhysRev.34.03.425
9. X.P. Zhang, Z.Z. Ren, Q.J. Zhi et al., Systematics of β^{-}-decay half-lives of nuclei far from the β-stable line. J. Phys. G: Nucl. Part. Phys. **34**, 2611 (2007). https://doi.org/10.1088/0954-3899/34/12/007
10. T. Tachibana, M. Yamada, and Y. Yoshida, Improvement of the gross theory of β-decay. II: One-particle strength function. Prog. Theor. Phys. **84**, 641 (1990). https://doi.org/10.1143/PTP.84.641
11. K. Takahashi, M. Yamada, Gross theory of nuclear β-decay. Prog. Theor. Phys. **41**, 1470 (1969). https://doi.org/10.1143/PTP.41.1470
12. H. Nakata, T. Tachibana, M. Yamada, Gross theory of nuclear β-decay. Nucl. Phys. A **625**, 521 (1997). https://doi.org/10.1016/S0375-9474(97)00413-2
13. J.Y. Fang, J. Chen, Z.M. Niu, Gross theory of β decay by considering the spin-orbit splitting from relativistic Hartree-Bogoliubov theory. Phys. Rev. C **106**, 054318 (2022). https://doi.org/10.1103/PhysRevC.106.054318
14. K. Langanke, G. Martínez-Pinedo, Nuclear weak-interaction processes in stars. Rev. Mod. Phys. **75**, 819 (2003). https://doi.org/10.1103/RevModPhys.75.819
15. B.R. Barrett, Microscopic calculations of nuclear structure beyond the 0p-shell. J. Phys. Conf. Ser. **445**, 012002 (2013). https://doi.org/10.1088/1742-6596/445/1/012002
16. K. Langanke, E. Kolbe, D.J. Dean, Unblocking of the Gamow-Teller strength in stellar electron capture on neutron-rich germanium isotopes. Phys. Rev. C **63**, 032801(R) (2001). https://doi.org/10.1103/PhysRevC.63.032801
17. T. Suzuki, T. Yoshida, T. Kajino et al., β decays of isotones with neutron magic number of N=126 and *r*-process nucleosynthesis. Phys. Rev. C **85**, 015802 (2012). https://doi.org/10.1103/PhysRevC.85.015802
18. Q. Zhi, E. Caurier, J.J. Cuenca-García et al., Shell-model half-lives including first-forbidden contributions for *r*-process waiting-point nuclei. Phys. Rev. C **87**, 025803 (2013). https://doi.org/10.1103/PhysRevC.87.025803
19. Z.M. Niu, Y.F. Niu, H.Z. Liang et al., β-decay half-lives of neutron-rich nuclei and matter flow in the *r*-process. Phys. Lett. B **723**, 172 (2013). https://doi.org/10.1016/j.physletb.2013.04.048
20. J. Engel, M. Bender, J. Dobaczewski et al., β decay rates of *r*-process waiting-point nuclei in a self-consistent approach. Phys. Rev. C **60**, 014302 (1999). https://doi.org/10.1103/PhysRevC.60.014302
21. D.D. Ni, Z.Z. Ren, β-decay rates of neutron-rich Zr and Mo isotopes in the deformed quasiparticle random-phase approximation with realistic interactions. Phys. Rev. C **89**, 064320 (2014). https://doi.org/10.1103/PhysRevC.89.064320
22. P. Sarriguren, β-decay properties of neutron-rich rare-earth isotopes. Phys. Rev. C **95**, 014304 (2017). https://doi.org/10.1103/PhysRevC.95.014304
23. K. Yoshida, Naturalness, conformal symmetry, and duality. Prog. Theor. Exp. Phys. **11**, 113D02 (2013). https://doi.org/10.1093/ptep/ptt098
24. F. Minato, C.L. Bai, Impact of tensor force on β decay of magic and semimagic nuclei. Phys. Rev. Lett. **110**, 122501 (2013). https://doi.org/10.1103/PhysRevLett.110.122501
25. Z.Y. Wang, Y.F. Niu, Z.M. Niu et al., Nuclear β-decay half-lives in the relativistic point-coupling model. J. Phys. G Nucl. Part. Phys. **43**, 045108 (2016). https://doi.org/10.1088/0954-3899/43/4/045108
26. T. Marketin, L. Huther, G. Martínez-Pinedo, Large-scale evaluation of β-decay rates of *r*-process nuclei with the inclusion of first-forbidden transitions. Phys. Rev. C **93**, 025805 (2016). https://doi.org/10.1103/PhysRevC.93.025805
27. Y.F. Niu, Z.M. Niu, G. Colò et al., Interplay of quasiparticle-vibration coupling and pairing correlations on β-decay half-lives. Phys. Lett. B **780**, 325 (2018). https://doi.org/10.1016/j.physletb.2018.02.061
28. Y. F. Niu, G. Colò, E. Vigezzi *et al.*, Quasiparticle random-phase approximation with quasiparticle-vibration coupling: Application to the Gamow-Teller response of the superfluid nucleus ^{120}Sn., Phys. Rev. C **94**, 064328 (2016). https://doi.org/10.1103/PhysRevC.94.064328
29. Y.F. Niu, Z.M. Niu, G. Colò et al., Particle-vibration coupling effect on the β decay of magic nuclei. Phys. Rev. Lett. **114**, 142501 (2015). https://doi.org/10.1103/PhysRevLett.114.142501
30. P. Möller, J.R. Nix, K.-L. Kratz, Nuclear properties for astrophysical and radioactive ion-beam applications. At. Data Nucl. Data Tables **66**, 131 (1997). https://doi.org/10.1006/adnd.1997.0746
31. P. Möller, B. Pfeiffer, K.-L. Kratz, New calculations of gross β-decay properties for astrophysical applications: Speeding-up the

classical r process. Phys. Rev. C **67**, 055802 (2003). https://doi.org/10.1103/PhysRevC.67.055802
32. P. Möller, A.J. Sierk, T. Ichikawa et al., Nuclear ground-state masses and deformations: FRDM(2012). At. Data Nucl. Data Tables **109–110**, 1 (2016). https://doi.org/10.1016/j.adt.2015.10.002
33. P. Möller, M.R. Mumpower, T. Kawano et al., Nuclear properties for astrophysical and radioactive-ion-beam applications (II). At. Data Nucl. Data Tables **125**, 1 (2019). https://doi.org/10.1016/j.adt.2018.03.003
34. W.B. He, Q.F. Li, Y.G. Ma et al., Machine learning in nuclear physics at low and intermediate energies. Sci. China Phys. Mech. Astron. **66**, 282001 (2023). https://doi.org/10.1007/s11433-023-2116-0
35. Z.M. Niu, H.Z. Liang, Nuclear mass predictions based on Bayesian neural network approach with pairing and shell effects. Phys. Lett. B **778**, 48 (2018). https://doi.org/10.1016/j.physletb.2018.01.002
36. R. Utama, J. Piekarewicz, H.B. Prosper, Nuclear mass predictions for the crustal composition of neutron stars: A Bayesian neural network approach. Phys. Rev. C **93**, 014311 (2016). https://doi.org/10.1103/PhysRevC.93.014311
37. Z.M. Niu, H.Z. Liang, Nuclear mass predictions with machine learning reaching the accuracy required by *r*-process studies. Phys. Rev. C **106**, L021303 (2022). https://doi.org/10.1103/PhysRevC.106.L021303
38. X.H. Wu, L.H. Guo, P.W. Zhao, Nuclear masses in extended kernel ridge regression with odd-even effects. Phys. Lett. B **819**, 136387 (2021). https://doi.org/10.1016/j.physletb.2021.136387
39. H.F. Zhang, L.H. Wang, J.P. Yin et al., Performance of the Levenberg-Marquardt neural network approach in nuclear mass prediction. J. Phys. G **44**, 045110 (2017). https://doi.org/10.1088/1361-6471/aa5d78
40. L. Neufcourt, Y.C. Cao, W. Nazarewicz et al., Neutron drip line in the Ca region from Bayesian model averaging. Phys. Rev. Lett. **122**, 062502 (2019). https://doi.org/10.1103/PhysRevLett.122.062502
41. Z.Y. Yuan, D. Bai, Z. Wang et al., Reliable calculations of nuclear binding energies by the Gaussian process of machine learning. Nucl. Sci. Tech. **35**, 105 (2024). https://doi.org/10.1007/s41365-024-01463-9
42. R. Utama, W.-C. Chen, J. Piekarewicz, Nuclear charge radii: density functional theory meets Bayesian neural networks. J. Phys. G Nucl. Part. Phys. **43**, 114002 (2016). https://doi.org/10.1088/0954-3899/43/11/114002
43. Y.F. Ma, C. Su, J. Liu et al., Predictions of nuclear charge radii and physical interpretations based on the naive Bayesian probability classifier. Phys. Rev. C **101**, 014304 (2020). https://doi.org/10.1103/PhysRevC.101.014304
44. D. Wu, C.L. Bai, H. Sagawa et al., Calculation of nuclear charge radii with a trained feed-forward neural network. Phys. Rev. C **102**, 054323 (2020). https://doi.org/10.1103/PhysRevC.102.054323
45. T.S. Shang, J. Li, Z.M. Niu, Prediction of nuclear charge density distribution with feedback neural network. Nucl. Sci. Tech. **33**, 153 (2022). https://doi.org/10.1007/s41365-022-01140-9
46. T.S. Shang, H.H. Xie, J. Li et al., Global prediction of nuclear charge density distributions using a deep neural network. Phys. Rev. C **110**, 014308 (2024). https://doi.org/10.1103/PhysRevC.110.014308
47. L. Tang, Z.H. Zhang, Nuclear charge radius predictions by kernel ridge regression with odd-even effects. Nucl. Sci. Tech. **35**, 19 (2024). https://doi.org/10.1007/s41365-024-01379-4
48. Z.A. Wang, J.C. Pei, Y. Liu et al., Bayesian evaluation of incomplete fission yields. Phys. Rev. Lett. **123**, 122501 (2019). https://doi.org/10.1103/PhysRevLett.123.122501
49. C.Y. Qiao, J.C. Pei, Z.A. Wang et al., Bayesian evaluation of charge yields of fission fragments of ^{239}U. Phys. Rev. C **103**, 034621 (2021). https://doi.org/10.1103/PhysRevC.103.034621
50. J.H. Bai, Z.M. Niu, B.Y. Sun et al., The description of giant dipole resonance key parameters with multitask neural networks. Phys. Lett. B **815**, 136147 (2021). https://doi.org/10.1016/j.physletb.2021.136147
51. X.H. Wang, L. Zhu, J. Su, Providing physics guidance in Bayesian neural networks from the input layer: The case of giant dipole resonance predictions. Phys. Rev. C **104**, 034317 (2021). https://doi.org/10.1103/PhysRevC.104.034317
52. R.-D. Lasseri, D. Regnier, J.P. Ebran et al., Taming nuclear complexity with a committee of multilayer neural networks. Phys. Rev. Lett. **124**, 162502 (2020). https://doi.org/10.1103/PhysRevLett.124.162502
53. Y.F. Wang, X.Y. Zhang, Z.M. Niu et al., Study of nuclear low-lying excitation spectra with the Bayesian neural network approach. Phys. Lett. B **830**, 137154 (2022). https://doi.org/10.1016/j.physletb.2022.137154
54. W.B. He, Y.G. Ma, L.G. Pang et al., High-energy nuclear physics meets machine learning. Nucl. Sci. Tech. **34**, 88 (2023). https://doi.org/10.1007/s41365-023-01233-z
55. B.S. Cai, C.X. Yuan, Random forest-based prediction of decay modes and half-lives of superheavy nuclei. Nucl. Sci. Tech. **34**, 204 (2023). https://doi.org/10.1007/s41365-023-01354-5
56. Y.D. Zeng, J. Wang, R. Zhao et al., Decomposition of fissile isotope antineutrino spectra using convolutional neural network. Nucl. Sci. Tech. **34**, 79 (2023). https://doi.org/10.1007/s41365-023-01229-9
57. Y.F. Gao, B.S. Cai, C.X. Yuan, Investigation of β-decay half-life and delayed neutron emission with uncertainty analysis. Nucl. Sci. Tech. **34**, 9 (2023). https://doi.org/10.1007/s41365-022-01153-4
58. P.X. Du, T.S. Shang, K.P. Geng et al., Inference of parameters for the back-shifted Fermi gas model using a feedforward neural network. Phys. Rev. C **109**, 044325 (2024). https://doi.org/10.1103/PhysRevC.109.044325
59. Z. P. Gao, and Q. F. Li, Studies on several problems in nuclear physics by using machine learning. Nucl. Tech. (in Chinese) **46**, 080009 (2023). https://doi.org/10.11889/j.0253-3219.2023.hjs.46.080009
60. F. P. Li, L. G. Pang, and X. N. Wang, Application of machine learning to the study of QCD transition in heavy ion collisions. Nucl. Tech. (in Chinese) **46**, 040014 (2023). https://doi.org/10.11889/j.0253-3219.2023.hjs.46.040014
61. J. Zhou, J. Xu, Bayesian inference of neutron-skin thickness and neutron-star observables based on effective nuclear interactions. Sci. China Phys. Mech. Astron. **67**, 282011 (2024). https://doi.org/10.1007/s11433-024-2406-4
62. R. Wang, Y.G. Ma, R. Wada et al., Nuclear liquid-gas phase transition with machine learning. Phys. Rev. Res. **2**, 043202 (2020). https://doi.org/10.1103/PhysRevResearch.2.043202
63. Y.D. Song, R. Wang, Y.G. Ma et al., Determining the temperature in heavy-ion collisions with multiplicity distribution. Phy. Lett. B **814**, 136084 (2021). https://doi.org/10.1016/j.physletb.2021.136084
64. N.J. Costiris, E. Mavrommatis, K.A. Gernoth et al., Decoding β-decay systematics: A global statistical model for β^- half-lives. Phys. Rev. C **80**, 044332 (2009). https://doi.org/10.1103/PhysRevC.80.044332
65. Z.M. Niu, H.Z. Liang, B.H. Sun et al., Predictions of nuclear β-decay half-lives with machine learning and their impact on *r*-process nucleosynthesis. Phys. Rev. C **99**, 064307 (2019). https://doi.org/10.1103/PhysRevC.99.064307
66. F. Minato, Z.M. Niu, H.Z. Liang, Calculation of β-decay half-lives within a Skyrme-Hartree-Fock-Bogoliubov energy density functional with the proton-neutron quasiparticle random-phase approximation and isoscalar pairing strengths optimized by a Bayesian method. Phys. Rev. C **106**, 024306 (2022). https://doi.org/10.1103/PhysRevC.106.024306

67. W.F. Li, X.Y. Zhang, Y.F. Niu et al., Comparative study of neural network and model averaging methods in nuclear β-decay half-life predictions. J. Phys. G Nucl. Part. Phys. **51**, 015103 (2024). https://doi.org/10.1088/1361-6471/ad0314
68. P. Li, J.H. Bai, Z.M. Niu et al., β-decay half-lives studied using neural network method. Sci. China Phys. Mech. Astron. **52**, 252006 (2022). https://doi.org/10.1360/SSPMA-2021-0299
69. E.M. Ney, J. Engel, T. Li et al., Global description of β^- decay with the axially deformed Skyrme finite-amplitude method: Extension to odd-mass and odd-odd nuclei. Phys. Rev. C **102**, 034326 (2020). https://doi.org/10.1103/PhysRevC.102.034326
70. X. Glorot, Y. Bengio, Understanding the difficulty of training deep feedforward neural networks. Proc. Mach. Learn **9**, 249 (2010). https://doi.org/10.5555/3157382.3157509
71. A.E. Hoerl, R.W. Kennard, Ridge regression: Applications to nonorthogonal problems. Technometrics **12**, 69 (1970). https://doi.org/10.2307/1267352
72. A.E. Hoerl, R.W. Kennard, Ridge regression: Biased estimation for nonorthogonal problems. Technometrics **12**, 55 (1970). https://doi.org/10.1080/00401706.1970.10488699
73. M. Wang, W. J. Huang, F. G. Kondev *et al*., The AME 2020 atomic mass evaluation (II). Tables, graphs and references. Chin. Phys. C **45**, 030003 (2021). https://doi.org/10.1088/1674-1137/abddaf
74. J. Liu, Y.F. Niu, W.H. Long, New magicity $N = 32$ and 34 due to strong couplings between Dirac inversion partners. Phys. Lett. B **806**, 135524 (2020). https://doi.org/10.1016/j.physletb.2020.135524
75. G. Lorusso, S. Nishimura, Z.Y. Xu et al., β-decay half-lives of 110 neutron-rich nuclei across the $N = 82$ shell gap: Implications for the mechanism and universality of the astrophysical r process. Phys. Rev. Lett. **114**, 192501 (2015). https://doi.org/10.1103/PhysRevLett.114.192501
76. N. Wang, M. Liu, X.Z. Wu et al., Surface diffuseness correction in global mass formula. Phys. Lett. B **734**, 215 (2014). https://doi.org/10.1016/j.physletb.2014.05.049